

# Distributional Modeling for Location-Aware Adversarial Patches

Xingxing Wei, Shouwei Ruan, Yinpeng Dong, and Hang Su

**Abstract**—Adversarial patch is one of the important forms of performing adversarial attacks in the physical world. To improve the naturalness and aggressiveness of existing adversarial patches, location-aware patches are proposed, where the patch’s location on the target object is integrated into the optimization process to perform attacks. Although it is effective, efficiently finding the optimal location for placing the patches is challenging, especially under the black-box attack settings. In this paper, we propose the Distribution-Optimized Adversarial Patch (DOPatch), a novel method that optimizes a multimodal distribution of adversarial locations instead of individual ones. DOPatch has several benefits: Firstly, we find that the locations’ distributions across different models are pretty similar, and thus we can achieve efficient query-based attacks to unseen models using a distributional prior optimized on a surrogate model. Secondly, DOPatch can generate diverse adversarial samples by characterizing the distribution of adversarial locations. Thus we can improve the model’s robustness to location-aware patches via carefully designed Distributional-Modeling Adversarial Training (DOP-DMAT). We evaluate DOPatch on various face recognition and image recognition tasks and demonstrate its superiority and efficiency over existing methods. We also conduct extensive ablation studies and analyses to validate the effectiveness of our method and provide insights into the distribution of adversarial locations.

**Index Terms**—Adversarial Robustness, Physical Attacks, Location-aware Patches, Adversarial Patches, Adversarial Training

## 1 INTRODUCTION

VISUAL systems based on deep neural networks are vulnerable to adversarial examples [15], [44]. Previous works have striven to explore the robustness of visual models under the  $L_p$ -norms adversarial examples [5], [13], [25], [33], which deceive the model by adding small perturbations to input samples. However, in the physical world, adversarial patch attacks constrained to a localized region are more commonly encountered. In many computer vision tasks, such as face recognition, adversarial patch attacks are often executed by objects accompanying the human’s face (e.g., glasses [40], [41], masks [55], hats [24], etc.) or using an optimized patch with or without semantic information [4], [26], [27], [48], [49]. Such attacks are more threatening and easier to execute in the physical world, and can also be inconspicuous, thus posing a significant challenge to applying deep networks in security-critical applications. Therefore, evaluating and enhancing the robustness of visual models against adversarial patches is essential.

Generating adversarial patches involves optimizing unrestricted perturbations within localized regions. Traditional adversarial patches usually aim at optimizing perturbations while fixing the position of the object. Although regularization measures, such as Total Variance (TV) loss and Non-Printability Score (NPS) loss [24], [41], are incorporated to enhance the robustness and smoothness of adversarial perturbations, these attacks remain less natural, easily de-

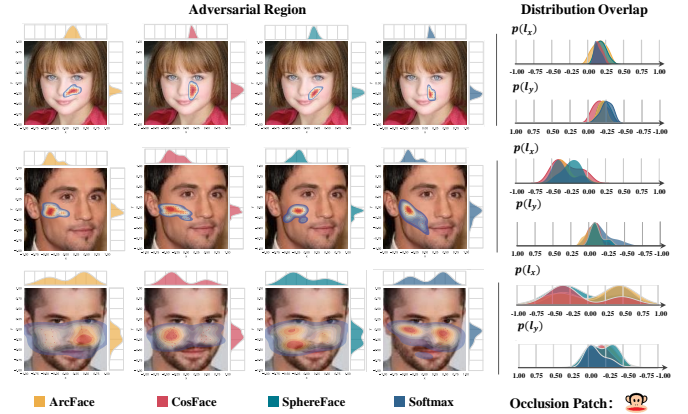


Fig. 1. When the patch is applied on the faces, the adversarial locations are regional aggregation (left) and the distributions are pretty similar across models (right). To ensure passing live detection, we mask the regions of facial features when optimizing adversarial locations like [48].

tectable, and defensible due to the local semantic deficit caused by the unrestricted perturbations [8], [38], [50]. To achieve both natural and aggressive patches, recent studies investigate the impact of the patch’s location [27], [38], [48], [49], [52], which is called location-aware adversarial patches in our paper. Location-aware patches are flexible, they can not only combine with the fixed pattern to construct the natural and stealthy physical attack (e.g., adversarial sticker in [48]) but also conduct the joint optimization with the traditional patches to improve their attack performance (e.g., [27], [49], etc.). For these reasons, location-aware patches deserve further investigation.

Despite the vulnerability of models to such location-aware patch attacks, current methods have certain limitations. For example, a recent observation [48] reveals that

- Xingxing Wei and Shouwei Ruan are with the Institute of Artificial Intelligence, Beihang University, No.37, Xueyuan Road, Haidian District, Beijing, 100191, P.R. China. (E-mail: shouweiruan, xxwei@buaa.edu.cn).
- Yinpeng Dong and Hang Su are with the Institute for Artificial Intelligence, Beijing National Research Center for Information Science and Technology, Department of Computer Science and Technology, Tsinghua University, Beijing 100084, China.
- Corresponding author: Xingxing Wei.

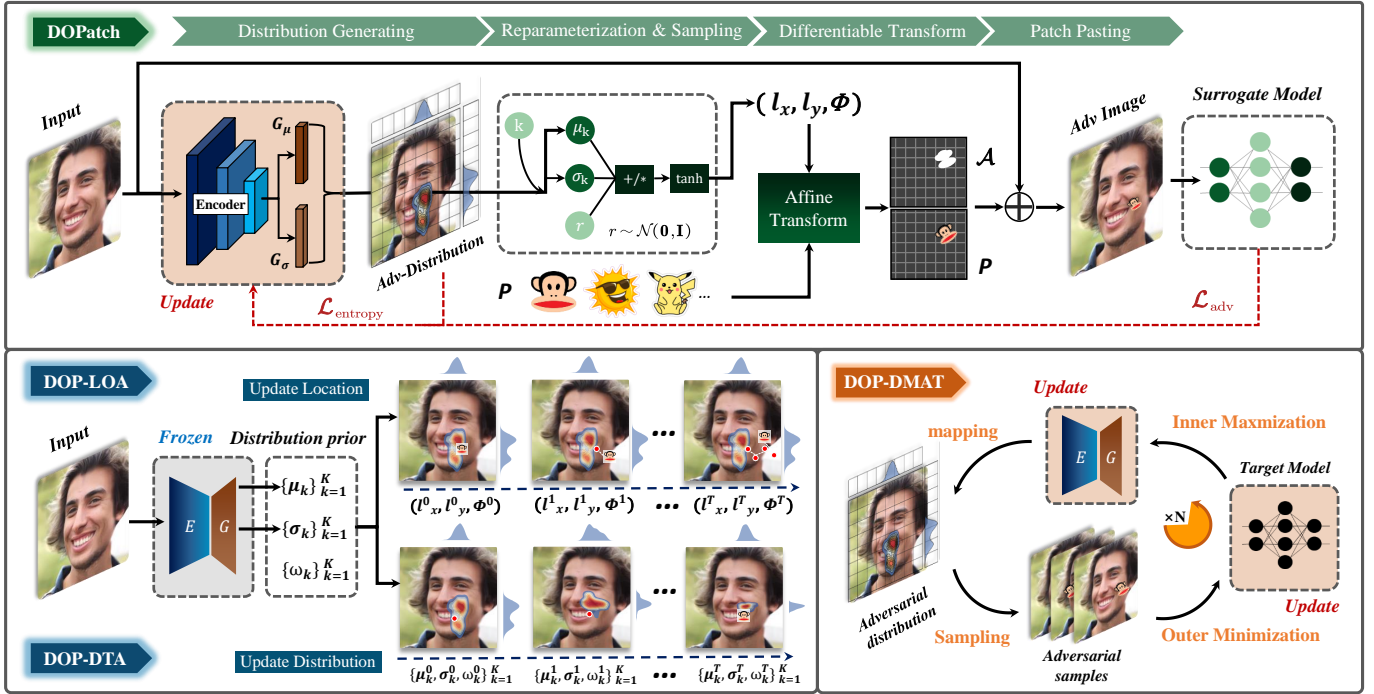


Fig. 2. The overview of our method. The first stage (DOPatch) is carried out on the surrogate model to optimize a distribution mapping network. It maps the image input to the corresponding distribution parameters of the adversarial location. The second stage is to conduct attacks (DOP-LOA and DOP-DTA) or defense (DOP-DMAT) leveraging the distributional prior. To better show the effect of the distribution-optimized modeling method in our paper, we adopt the same setting in [48] and only optimize the patch’s location for the fixed meaningful pattern. Thus, we can focus on location optimization and don’t need to consider the pattern’s influence.

adversarial locations of fixed patterns exhibit significant regional aggregation, as shown in Fig. 1, where the colorful regions on the faces denote the adversarial locations to show effective attacks. We see that the positions that can lead to successful attacks are not discretely distributed but clustered in some specific regions. Due to this phenomenon, the main limitation is that existing methods concentrate solely on optimizing a single location [27], [48], [49] and neglect their intrinsic distribution property, thus leading to inadequate modeling to characterize the aggregation regions of the adversarial locations, and further restricting its potential function on attack efficiency and defense effects.

To address these problems, in this paper, we propose **Distribution-Optimized Adversarial Patch (DOPatch)**, a novel method to search for the worst-case placement region in a distributional modeling manner. Specifically, DOPatch optimizes a multimodal distribution of adversarial locations instead of individual ones to characterize the multiple regions, which can provide several benefits. Firstly, we can achieve efficient query-based attacks on other unseen models using the distributional prior optimized on the surrogate model. It is based on our finding that although individual adversarial locations vary across models, there is a similarity in their distributions, as shown in Fig. 1. Secondly, DOPatch can generate adversarial samples with improved diversity by characterizing the distribution of adversarial locations. Thus, we can improve the model’s robustness to location-aware patches via adversarial training.

However, distributional modeling on the adversarial locations is challenging. A straightforward way is to exhaustively search for all the adversarial locations and then obtain the multimodal distribution via a statistical approach,

which is high-computation and time-consuming. For that, we propose a novel distribution mapping network, which maps the face images to their corresponding multimodal distribution parameters. The network is trained under the supervision of the designed adversarial loss (Eq.(8)) and entropy regularization loss (Eq.10), aiming to balance the aggressiveness and generalization of the adversarial distribution. To ensure gradient propagation throughout the pipeline, we employ differentiable affine transformations to map fixed-pattern patches and their masks to the specified locations in the object by considering the object’s surface change. The process is illustrated in Fig. 2 (top row).

After distributional modeling, we conduct the attack or defense leveraging the distributional transfer prior. Specifically, as for attack, we perform a query-based attack with few queries to target models, employing two distinct modes tailored to different mechanisms. The first one is **Location-Optimization Attack (DOP-LOA)**, which optimizes a single adversarial location starting from the center of the distributional prior. And the second one is **Distribution-Transfer Attack (DOP-DTA)**, which optimizes the distribution parameters to capture the adversarial region of the black-box target model precisely. Compared with DOP-LOA, DOP-DTA makes full use of the intrinsic distribution property of adversarial locations, and thus has better attack performance. The process is illustrated in Fig. 2 (bottom left).

As for defense, we utilize adversarial training to improve the model’s robustness to the existing location-aware patches. For that, we design a **Distributional-Modeling Adversarial Training (DOP-DMAT)**, which is formulated as a distribution-based min-max problem following the ADT [12], where the inner maximization aims to optimize

the distribution of adversarial location using DOPatch. And outer minimization aims to train a robustness model by minimizing the expected loss over the worst-case adversarial location distributions. By exploring the diverse adversarial locations sampling from the distribution, DOP-DMAT is suitable for training robust models. The process is illustrated in Fig. 2 (bottom right).

We conduct extensive experiments on the face recognition task and image recognition task to demonstrate the effectiveness of the proposed method. Experimental result shows that DOPatch characterizes the region of adversarial location and improves the attack’s effectiveness while reducing the number of queries, demonstrating better performance than previous methods. Based on it, DOP-DMAT significantly improves the robustness of face recognition models against location-aware patches. The code is available at <https://github.com/Heathcliff-saku/DOPatch>.

In summary, this paper has the following contributions:

(1) We propose the Distribution-Optimized Adversarial Patch (DOPatch), a novel framework that can efficiently search for the worst-case region of fixed-pattern patch locations. It aims to optimize a multimodal distribution of adversarial locations instead of individual location points.

(2) To evaluate the robustness of black-box visual systems with limited information. We further design two query-based attack modes using distribution prior: Location Optimization Attack (DOP-LOA) and Distribution Transfer Attack (DOP-DTA), which can perform effective attacks with only a few queries with the visual systems.

(3) We propose DOP-DMAT, a distribution-based adversarial training that employs DOPatch to address the inner maximization problem. By leveraging DOP-DMAT, we can significantly improve the robustness of the model against location-aware adversarial patches.

(4) We conduct extensive experiments on face recognition and image recognition tasks to verify the proposed methods. Specifically, we adopt DOPatch to perform attacks and defense on various face and image recognition models (including the popular big models). A variety of experiments show that our method achieves the best performance compared with the SOTA methods.

## 2 RELATED WORK

### 2.1 Adversarial Patch Attacks

The adversarial patch is originally proposed in [4] to fool deep networks in the physical world. It aims to optimize an unrestricted perturbation within a particular region of a clean image. Unlike imperceptible perturbations based on  $L_p$ -norms, adversarial patches are capturable and robust perturbations that can be applied effectively in physical attacks. The adversarial patches are widely adopted in various vision tasks, such as image recognition [4], [14], [22], [28], object detection [6], [26], [31], [46], semantic segmentation [35], [37], depth estimation [51], etc., posing a significant threat to the deployment of models in the physical world. Previous works propose several strategies to craft more robust patches, among which Expectation over Transformation (EOT) [2] is a commonly used method to improve the robustness of patches against rotation and scaling. To make adversarial patches more imperceptible,

Chindaudom et al. [9] propose the adversarial QR patch, which constrains patches to QR patterns. Additionally, Liu et al. [28] propose PS-GAN, the first GAN-based method to generate more natural-looking adversarial patches. Adversarial patches also threaten face recognition tasks, where the imperceptibility of patches is a more significant concern than other tasks, like Adv-Glasses [40], [41], Adv-Hat [24], Adv-masks [55], AT3D [53], etc. These methods mainly depend on optimizing the patch’s pattern to achieve attacks, thus we can call them as **pattern-aware adversarial patches**.

On the contrary, some studies aim at optimizing the patch’s location by using the fixed meaningful pattern to perform attacks. For example, RHDE [48] achieves the attack by optimizing the placement of an existing sticker. Not only obtaining the inferior in attack performance, it is also easy to implement, i.e., it can use common materials such as cartoon stickers as the fixed pattern. Inspired by these works, the joint pattern-location optimization methods are proposed. For example, Li et al. [27] generate the texture and location of patches using a generator network. Similarly, Wei et al. [49] propose a reinforcement learning framework for joint optimization of texture and location in a black-box setting. [38] performs pattern-location optimization via an iterative strategy. Because the patch’s location is integrated to conduct attacks, we call them as **location-aware adversarial patches**.

The summary for these related works is given in Fig. 3. While the location-aware adversarial patches show good performance, they are all limited to optimizing individual positions. In contrast, we aim to model the distribution of adversarial locations implicitly. This allows us to comprehensively characterize these regions and improve the performance and robustness of location-aware patches. Moreover, we can efficiently improve the model’s robustness against the patch through distribution-based adversarial training. To better show the effect of the distribution-optimized modeling method in our paper, we adopt the same setting in [48] and only optimize the patch’s location for the fixed pattern. Thus, we can focus on the location optimization, and don’t need to consider the pattern’s influence.

### 2.2 Defense for Adversarial Patches

Various methods have been proposed to defend against adversarial patches, which can be categorized into three stages: pre-processing, in-processing, and post-processing. Pre-processing methods apply some transformations to the input data to increase the model’s robustness. For example, removing [18], [29] or blurring [36] the patch in input images can mitigate the effect of adversarial attacks. In-processing methods use some techniques to reduce or avoid the impact of adversarial attacks during the model’s training phase, such as adversarial training [34], [38]. Post-processing methods process the model’s output to correct the wrong prediction. For instance, [17] adjusts the predicted probabilities to a more balanced distribution to ensure correct prediction.

Our method belongs to the in-processing stage. But different from the existing methods [34], [38] that utilize pattern-aware adversarial patches to perform adversarial training, we use location-aware adversarial patches, and furthermore conduct adversarial distribution training, which can achieve better defense performance.

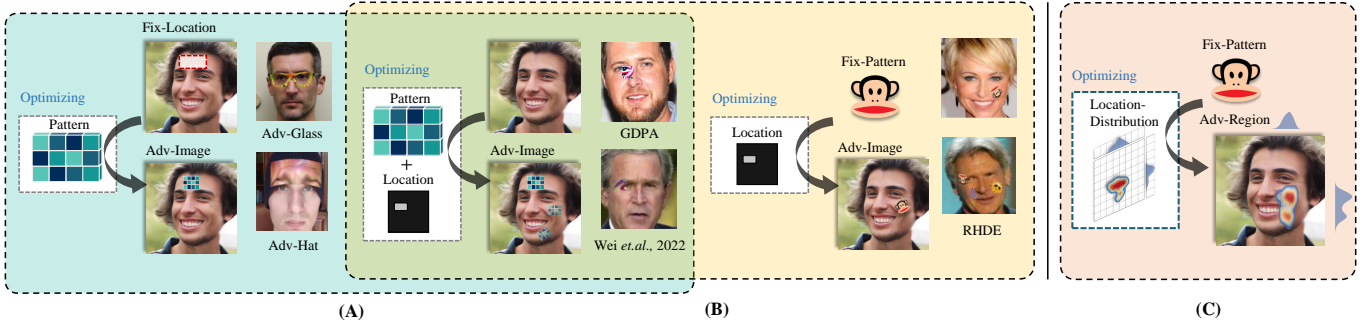


Fig. 3. The summary of the existing adversarial patch attacks in face recognition: previous works can be divided into (A) **pattern-aware patches** and (B) **location-aware patches**. In this paper, we propose a new approach which optimizes the distribution of adversarial locations to improve the performance of location-aware patches, as shown in (C).

### 3 METHODOLOGY

This section first introduces the distributional transferability of adversarial locations in Sec. 3.1. Based on this finding, we formulate the problem in Sec. 3.2 and present the distributional modeling and black-box attacks in Sec. 3.3 and Sec. 3.4. Finally, we give the adversarial training method in Sec. 3.5. An overview of our framework is shown in Fig. 2.

#### 3.1 Distributional Transferability

Previous work finds that adversarial locations have regional aggregation when a fixed patch pattern’s perturbations is given [48], [49]. We further investigate the distribution of these aggregate locations for the same sample across different models and discover an interesting phenomenon: **the distributions of adversarial locations on different models partially overlap, indicating that there exists a cross-model transferability in the distribution of adversarial locations.**

To verify this hypothesis, we first devise a preliminary experiment to observe the distribution of adversarial locations and explore their transferability. Specifically, the face classification task serves as an example, where we begin by grid-traversing each location in an image sample  $\mathbf{X}$  to capture the corresponding adversarial locations  $\theta = (l_x, l_y)$  causing successful attacks. Next, we use kernel density estimation (KDE) to carve the joint probability density  $p(\theta)$  for the given  $\mathbf{X}$ , w.r.t various face classifiers that are trained with different loss functions, including ArcFace [11], CosFace [47], SphereFace [30] and Softmax [43], [45]. The visualization for a face image is shown in Fig. 1 (left), where we observe that the joint distributions  $p(\theta)$  across different models exhibit high similarity. To illustrate this point more visually, we also depict the marginal distributions  $p(l_x)$ ,  $p(l_y)$  in Fig. 1 (right), highlighting their significant overlap. We conduct experiments on 100 face images randomly selected from LFW dataset, and the similar phenomenon occurs on all the samples. This observation inspires the idea that if we can optimize the distribution of adversarial locations in surrogate models, we can leverage its cross-model transfer prior to perform efficient query-based black-box attacks [1]. To this end, we propose two methods to optimize the distribution of adversarial locations, which are detailed in Sec. 3.4. Besides, because  $p(\theta)$  captures the diversity of adversarial locations, we can perform an effective

adversarial training using the diverse adversarial locations sampling from the distribution, details are given in Sec. 3.5.

#### 3.2 Problem Formulation

In visual recognition, the adversarial attack aims to apply a perturbation to the clean image  $\mathbf{X}$  to make the model predict incorrectly. For the  $L_p$ -norms attack, the perturbation  $\delta$  is added to each pixel over the entire image, formulated as  $\mathbf{X}^{adv} = \mathbf{X} + \delta$ . In contrast, the perturbation of the adversarial patch is limited to a particular shape and location:

$$\mathbf{X}^{adv} = (1 - \mathcal{A}) \odot \mathbf{X} + \mathcal{A} \odot \delta, \quad (1)$$

where  $\mathcal{A} \in \{0, 1\}^{w \times h}$  is a binary matrix to mask the patch area and  $\odot$  represents the Hadamard product. The pattern-aware methods focus on optimizing the patch perturbation  $\delta$  with a pre-fixed  $\mathcal{A}$ . In contrast, the location-aware methods do not generate  $\delta$  but choose a fixed pattern as perturbations, such as cartoon stickers [48], and fix the shape of  $\mathcal{A}$ , while trying to optimize the pasting location to generate adversarial patch samples as follows:

$$\mathbf{X}^{adv} = (1 - T(\mathcal{A}, \theta)) \odot \mathbf{X} + T(\mathcal{A}, \theta) \odot \mathbf{P}, \quad (2)$$

where  $\mathbf{P}$  is the fixed pattern,  $T(\cdot)$  is the affine transform operator, and  $\theta = [l_x, l_y, \phi]$  represents the affine transformation parameters, where  $l_x$  and  $l_y$  are the pattern translation along the x and y axes, and  $\phi$  is the pattern rotation. For simplicity, we define  $\mathcal{G}(\mathbf{X}, \mathbf{P}, \theta)$  as the process of generating adversarial samples using the location-aware patch.

Unlike previous methods searching for a single adversarial location  $\theta$ , the proposed DOPatch captures the aggregated regions of the adversarial locations using a distribution  $p(\theta)$ . By optimizing the  $p(\theta)$  under proper parameterization, most  $\theta$  sampled from it is likely to mislead the model, and we can use  $p(\theta)$  for effective query-based attacks. Thus, based on Eq. (2), we formulate DOPatch as solving the following optimization problem:

$$\max_{p(\theta)} \{ \mathbb{E}_{p(\theta)} [\mathcal{L}(\mathcal{G}(\mathbf{X}, \mathbf{P}, \theta))] - \lambda \cdot \log p(\theta) \}, \quad (3)$$

where  $\mathcal{L}(\cdot)$  is the adversarial loss (e.g. cross-entropy loss in classification task) that will be specifically defined in Sec. 3.3,  $-\log p(\theta)$  is the negative log density, whose expectation is the distribution’s entropy, we use it as a regularization loss to avoid the optimal distribution degenerate

into a Dirac one [12].  $\lambda$  is the balance parameter between adversarial and entropy losses.

As shown in Eq. (3), DOPatch aims to optimize the worst-case distribution of adversarial locations by maximizing the loss expectation. The motivation for using  $p(\theta)$  instead of individual  $\theta$  is multifaceted. *Firstly*, as explored in Sec. 3.1, using distribution prior can carry out efficient query-based attacks due to its cross-model transferability prior. *Secondly*, learning the underlying distribution to explore the adversarial location region can better help us understand the model’s vulnerabilities.

### 3.3 Distribution-Optimized Adversarial Patch

#### 3.3.1 Parameterization of Location Distributions

A natural approach to solving Eq. (3) is to use trainable parameters to parameterize the adversarial distribution  $p(\theta)$ . Since the loss landscape w.r.t adversarial locations exhibits multiple local maximal regions, we expect the optimized  $p(\theta)$  to be able to capture the adversarial locations comprehensively. Previous works, such as Adversarial Distributional Training (ADT) [12], use the uni-modal Gaussian distribution to parameterize the adversarial distribution of the  $L_p$ -norms perturbation. However, the uni-modal Gaussian distribution is insufficient to characterize multiple local maximals. To overcome this problem, we use multimodal Gaussian distribution as the parametric representation of  $p(\theta)$ , which learns multiple Gaussian components to cover different local maximals of the loss landscape.

Specifically, we parameterize  $p(\theta)$  by a mixture of  $K$  Gaussian components, in which the distribution parameters are denoted as  $\Psi = \{\mu_k, \sigma_k, \omega_k\}_{k=1}^K$ . The  $\mu_k \in \mathbb{R}^3$  and  $\sigma_k \in \mathbb{R}^3$  are the mean and standard deviation of  $k$ -th Gaussian component. The  $\omega_k \in [0, 1]$  ( $\sum_{k=1}^K \omega_k = 1$ ) represents the weights of components. To ensure that  $\theta$  is bounded within the range  $[-1, 1]$  allowed by the affine transformation matrix, we further employ the transformation of the random variable approach. Eventually,  $p(\theta)$  is parameterized as:

$$\theta = \tanh(\mathbf{u}/\tau), \text{ with } p(\mathbf{u}|\Psi) = \sum_{k=1}^K \omega_k \cdot \mathcal{N}(\mathbf{u}|\mu_k, \sigma_k^2 \mathbf{I}), \quad (4)$$

where  $\tau$  is a hyperparameter controlling the slope of  $\tanh$ . As shown in Eq. (4), location  $\theta$  is obtained by  $\tanh$  transformation of intermediate variables  $\mathbf{u}$  for normalization, while  $\mathbf{u}$  follows a multi-modal Gaussian distribution. Note that  $p(\mathbf{u}|\Psi)$  is now in a summation form, which is not convenient for computing the gradient. Therefore, we rewrite  $p(\mathbf{u}|\Psi)$  into a multiplication form:

$$p(\mathbf{u}|\Psi) = \sum_{\Gamma} p(\mathbf{u}, \Gamma|\Psi), \quad (5)$$

where  $p(\mathbf{u}, \Gamma|\Psi) = \prod_{k=1}^K \omega_k^{\gamma_k} \cdot \mathcal{N}(\mathbf{u}|\mu_k, \sigma_k^2 \mathbf{I})^{\gamma_k}$ ,

where  $\Gamma = \{\gamma_k\}_{k=1}^K$  is a latent one-hot vector introduced to determine which component the sampled location belongs to and obeys a multinomial distribution with probability  $\omega_k$ . Given the  $p(\mathbf{u}|\Psi)$  parameterized by Eq. (5), the optimization problem in Eq. (3) is appropriately rewritten as:

$$\max_{\Psi} \left\{ \mathbb{E}_{p(\mathbf{u}, \Gamma|\Psi)} [\mathcal{L}(\mathcal{G}(\mathbf{X}, \mathbf{P}, \tanh(\mathbf{u}/\tau))] - \lambda \cdot \log p(\tanh(\mathbf{u}/\tau)) \right\}. \quad (6)$$

To solve Eq. (6), we adopt gradient-based methods to obtain optimized distribution parameters  $\Psi$ , which will be given in the next section.

#### 3.3.2 Distribution Mapping Network

While it is possible to directly optimize  $\Psi$  using gradient descent directly, in order to achieve greater attack efficiency and generalize the attack performance to unseen samples, we draw inspiration from prior work [27], [28] and propose a novel distribution mapping network, which aims to learn the mapping functions from clean samples to their corresponding adversarial location distribution parameters:

$$F_{\mathbf{W}} = \mathbf{X} \rightarrow \{\mu_k, \sigma_k\}_{k=1}^K, \quad (7)$$

where  $\mathbf{W}$  is the weight of the network. This method allows for the efficient optimization of  $\Psi$  in higher-dimensional parameter space and is capable of generalizing to unseen samples due to the learned mapping functions. Note that here we do not learn the component weights  $\omega_k$ . The reason is two-fold. First, in practice, the multi-modal distribution tends to degrade to the uni-modal case when  $\omega_k$  is optimizing, thus failing to capture heterogeneous adversarial locations. Second, since  $\omega_k$  will be used to sample latent variables  $\Gamma$  from multinomial distribution, this operation is non-differentiable and cannot be gradient-passed. Thus, we fix  $\omega_k=1/K$  and properly optimize them in the second stage.

We design the network based on an encoder-decoder architecture, where the encoder  $E$  extracts feature from the input image  $\mathbf{X}$ , the decoders  $G_{\mu}$ ,  $G_{\sigma}$  share the same latent features extracted by  $E$  and generate the corresponding means  $\{\mu_k\}_{k=1}^K$  and standard deviations  $\{\sigma_k\}_{k=1}^K$ . Specifically, we use two different encoder architectures to cope with different target models: ResNet-50 [19] and the architecture adapted from CycleGAN [54]. On the top of  $E$ , we use two fully-connected layers as the  $G_{\mu}$  and  $G_{\sigma}$ , respectively. After obtaining the distribution parameters by the distribution mapping network, we adopt the low-variance reparameterization trick [3], [23] to maintain the gradient information during follow-up sampling. Specifically, we reparameterize  $\mathbf{u}$  as  $\mathbf{u} = \prod_{k=1}^K \mu_k^{\gamma_k} + \prod_{k=1}^K \sigma_k^{\gamma_k} \cdot \mathbf{r}$ , where  $\mathbf{r} \sim \mathcal{N}(\mathbf{0}, \mathbf{I})$ . Thus, in the classification task, the first term in Eq. (6) (i.e., the adversarial loss) can be calculated as:

$$\mathcal{L}_{\text{adv}} = \mathcal{L}_{\text{CE}}(f(\mathcal{G}(\mathbf{X}, \mathbf{P}, \tanh(\prod_{k=1}^K \frac{\mu_k^{\gamma_k}}{\tau} + \prod_{k=1}^K \frac{\sigma_k^{\gamma_k} \cdot \mathbf{r}}{\tau})), t), \quad (8)$$

where  $f$  is the victim model,  $\mathcal{L}_{\text{CE}}$  is the cross-entropy loss, and  $t$  is the true label of the input image. Similarly, in the identification task, we define the adversarial loss as:

$$\mathcal{L}_{\text{adv}} = 1 - \cos(f(\mathcal{G}(\mathbf{X}, \mathbf{P}, \tanh(\prod_{k=1}^K \frac{\mu_k^{\gamma_k}}{\tau} + \prod_{k=1}^K \frac{\sigma_k^{\gamma_k} \cdot \mathbf{r}}{\tau})), f(\mathbf{X})), \quad (9)$$

where  $\cos(\cdot)$  is the cosine similarity. The second term in Eq. (6) (i.e., the entropy loss) can be calculated analytically as (proof in Appendix B.7):

$$\mathcal{L}_{\text{entropy}} = \sum_{k=1}^K \gamma_k \cdot \left[ -\omega_k + \frac{\mathbf{r}^2}{2} + \frac{\log(2\pi)}{2} + \log \sigma_k + \log(\tanh(\frac{\mu_k + \sigma_k \mathbf{r}}{\tau})^2 - 1) - \log \tau \right]. \quad (10)$$

By integrating two loss terms, the total objective of the distribution mapping network is:

$$\max_{\mathbf{W}} [\mathbb{E}_{\mathcal{N}(\mathbf{r}|\mathbf{0},\mathbf{I})} (\mathcal{L}_{\text{adv}} - \lambda \cdot \mathcal{L}_{\text{entropy}})], \quad (11)$$

In practice, we use the Monte Carlo method to approximate the expectation.

### 3.3.3 Differentiable Affine Transformation

The affine transformation is an essential step in generating location-aware adversarial patches, which involves transforming the fixed pattern to a specific location in the object by considering the object’s surface change. To achieve this, we define differentiable affine transform operators based on the approach presented in Spatial Transformer Networks (STN) [21]. In contrast to GDPA [27], which considers only translation, we incorporate rotation to expand the search space. Specifically, for a given location parameter  $\theta = [l_x, l_y, \phi] \in [-1, 1]^3$  (derived from Eq. (4)), we define the pixel index relation of the pattern before and after the affine transformation as:

$$\begin{Bmatrix} x_i^s \\ y_i^s \end{Bmatrix} = \begin{bmatrix} \cos(\frac{\phi \cdot \pi}{2}) & \sin(\frac{\phi \cdot \pi}{2}) & \frac{w \cdot l_x}{2} \\ -\sin(\frac{\phi \cdot \pi}{2}) & \cos(\frac{\phi \cdot \pi}{2}) & \frac{h \cdot l_y}{2} \end{bmatrix} \cdot \begin{Bmatrix} x_i^t \\ y_i^t \\ 1 \end{Bmatrix}, \quad (12)$$

where  $(x_i^s, y_i^s)$  is the pixel index of the original image while  $(x_i^t, y_i^t)$  is the corresponding index of the transformed image. To achieve a differentiable transformation, STN uses the bilinear interpolation method to sample the pixel values of the transformed image from the original image:

$$V_i^c = \sum_{h=1}^H \sum_{w=1}^W U_{hw}^c \max(0, 1 - |x_i^s - w|) \max(0, 1 - |y_i^s - h|), \quad (13)$$

where  $c$  denotes the colour channels,  $U_{hw}^c$  is the pixel value of the original image in the index  $(h, w)$ , and  $V_i^c$  is the pixel value of the transformed image in the index  $(x_i^t, y_i^t)$ . Thus, we can use differentiable affine transformations to simultaneously transform the fixed pattern and its corresponding mask, allowing the entire pipeline to backpropagate the loss.

### 3.3.4 Overview of Optimization Algorithms

As demonstrated in Fig. 2, the pipeline of our method is divided into two stages. The core of the first stage is to learn the distribution mapping network in a surrogate white-box model to obtain the distribution prior. Formally, given a dataset  $\mathcal{D} = \{(\mathbf{X}_i, t_i)\}_{i=1}^n$ , for each training epoch, we first obtain the distribution parameters corresponding to each image using the distribution mapping network. Then we sample a set of location parameters for each image using the Monte Carlo method, generate a set of adversarial samples by Eq. (2), feed them to the surrogate model, calculate the mean of losses, and backpropagate to update the distribution mapping network weights. Algorithm 1 outlines the optimization algorithm of DOPatch in the first stage.

## 3.4 Black-Box Attacks with Distributional Prior

To leverage the transferability of adversarial distribution priors, we further design two query-based attack methods based on the transfer-prior against black-box models, which involve fine-tuning for individual attack locations (Sec. 3.4.1) and fine-tuning the parameters of the adversarial distribution (Sec. 3.4.2). Details are shown in the following.

---

### Algorithm 1: Optimization Algorithms for DOPatch

---

**Input:** attack data  $\mathcal{D}$ , distribution mapping network  $F_{\mathbf{W}}$ , surrogate model  $f$ , training epochs  $N$ , components number  $K$ , Monte Carlo sample number  $Q$ , balance hyperparameter  $\lambda$ .

- 1 Initialize network weights  $\mathbf{W}$ ;
- 2  $\{\omega_k\}_{k=1}^K \leftarrow \frac{1}{K}$ ;
- 3 **for** epoch = 1 **to**  $N$  **do**
- 4     **for** each minibatch  $\mathcal{B} \subset \mathcal{D}$  **do**
- 5         /\* obtaining distribution parameters \*/
- 6          $\{\mu_k^*, \sigma_k^*\}_{k=1}^K \leftarrow F_{\mathbf{W}}(\mathcal{B})$ ;
- 7          $\mathcal{L} \leftarrow 0$ ;
- 8         /\* calculating loss expectations \*/
- 9         **for**  $q = 1$  **to**  $Q$  **do**
- 10             sample  $\mathbf{r}$  from  $\mathcal{N}(\mathbf{0}, \mathbf{1})$ ;
- 11             sample  $\Gamma$  from a multinomial distribution with probability  $\{\omega_k\}_{k=1}^K$ ;
- 12             calculate  $\mathcal{L}_{\text{adv}}$  and  $\mathcal{L}_{\text{entropy}}$  by Eq. (8), Eq. (9) and Eq. (10);
- 13              $\mathcal{L} \leftarrow \mathcal{L} + \frac{1}{Q} (\mathcal{L}_{\text{adv}} - \lambda \cdot \mathcal{L}_{\text{entropy}})$ ;
- 14         **end**
- 15         /\* updating network weights \*/
- 16         update  $\mathbf{W}$  with stochastic gradient ascent
- 17          $\mathbf{W} \leftarrow \mathbf{W} + \nabla_{\mathbf{W}} \mathcal{L}$ ;
- 18     **end**
- 19 **end**

**Output:** optimized network  $F_{\mathbf{W}^*}$

---

### 3.4.1 Location-Optimization Attack (DOP-LOA)

To search for an effective adversarial location with limited information, the general idea is to directly sample alternative locations from the distribution prior or use a grid traversal to search for feasible attack locations within the distribution prior range. However, these methods lack heuristics and result in low search efficiency. Additionally, they cannot overcome variations in the adversarial distribution between surrogate and black-box models. To address these issues, we propose to use the Bayesian Optimization Algorithm (BOA) [42] to better break the dilemma between exploration and exploitation for searching worst-case placement locations. BOA is an effective method to solve global optimization problems. It comprises two key components: a surrogate model (e.g., Gaussian Process) is employed to model the unknown objective function, and the acquisition function is utilized to determine the next sampling point from the Bayesian posterior. The selection of the acquisition function is critical as it balances the exploration and exploitation dilemmas in the optimization process.

To rationally apply the distribution prior, we limit the range of Bayesian optimization to the  $3\sigma$  range around the distribution prior center  $\mu$ . Specifically, we use a Gaussian Process (GP) as the surrogate model to fit the Bayesian posterior distribution of the unknown function  $\mathcal{L}_{\text{adv}}(\theta)$  under observation samples  $\mathcal{O}_N = \{\theta_i, \mathcal{L}_{\text{adv}}(\theta_i)\}_{i=1}^N$ :

$$p(\theta_{s+1} | \mathcal{O}_{N+s}) \sim \mathcal{N}(\tilde{\mu}_s(\theta_{s+1}), \tilde{\sigma}_s^2(\theta_{s+1})), \quad (14)$$

where  $s$  represents the number of iterations,  $\tilde{\mu}_s$  and  $\tilde{\sigma}_s^2$  is the mean and variance of the marginal distribution. Now, we can estimate the distribution that  $\theta_{s+1}$  obeyed at any value. Then, we use the Upper Confidence Bound of GP (GP-UCB) as the acquisition function (AC), which takes a weighted average of the mean and variance, and obtain the

next sampling point by maximizing the AC:

$$\theta_{s+1} \leftarrow \arg \max_{\theta_{s+1}} \alpha_{\text{GP-UCB}}(\theta_{s+1} | \mathcal{O}_{N+s}),$$

$$\text{where } \alpha_{\text{GP-UCB}}(\theta_{s+1} | \mathcal{O}_{N+s}) \leftarrow \tilde{\mu}_s(\theta_{s+1}) + \beta \cdot \tilde{\sigma}_s(\theta_{s+1}), \quad (15)$$

where  $\beta$  is a hyperparameter for balance exploration and exploitation. The overall algorithm is shown in Appendix, based on the objective function, we first obtain a batch of observation samples within the limited search space (i.e.,  $3\sigma$  space of the adversarial distribution prior) and initialize the GP model. In each iteration, we first maximize the AC to obtain the best next sampling point, add it to the observation sample set, and then update the GP model. Through multiple iterations of BOA, we heuristically explore the best attack location within the distribution prior.

### 3.4.2 Distribution-Transfer Attack (DOP-DTA)

Despite the ability of DOP-LOA to obtain specific adversarial locations under black-box models, it only generates a single adversarial sample per optimization process and cannot generalize to adversarial regions, which contradicts our original intention of using distribution modeling. To address this issue, we propose DOP-DTA, which aims to transfer the distribution prior from the surrogate model to the black-box model, thus enabling us to explore the model’s vulnerabilities despite having limited information while enhancing the performance of the attack. Therefore, we further optimize the distribution parameters under the black-box settings. Formally, DOP-DTA also aims to address Eq.(6) by utilizing the distribution prior generated by  $F_{\mathbf{W}^*}$ . However, the model’s structure and gradient information are unavailable now. Thus, we employ Natural Evolution Strategies (NES) to obtain the natural gradient of the adversarial loss w.r.t the distribution parameters. For the entropy regularization loss, we directly provide its analytical expression to compute the gradient. Accordingly, we can derive the total gradients of the objective function Eq.(6) w.r.t the distribution parameters, i.e., the  $\omega_k$ ,  $\mu_k$ , and  $\sigma_k$ , as follows:

$$\begin{aligned} \nabla_{\omega_k} &= \mathbb{E}_{\mathcal{N}(\mathbf{r}|0,\mathbf{I})} \left\{ \gamma_k \cdot \left[ \mathcal{L}_{\text{adv}} \cdot \frac{1}{\omega_k} - \lambda \right] \right\}, \\ \nabla_{\mu_k} &= \mathbb{E}_{\mathcal{N}(\mathbf{r}|0,\mathbf{I})} \left\{ \gamma_k \cdot \left[ \mathcal{L}_{\text{adv}} \cdot \frac{\sigma_k \mathbf{r}}{\omega_k} - \lambda \cdot 2 \tanh\left(\frac{\mu_k + \sigma_k \mathbf{r}}{\tau}\right) \cdot \frac{1}{\tau} \right] \right\}, \\ \nabla_{\sigma_k} &= \mathbb{E}_{\mathcal{N}(\mathbf{r}|0,\mathbf{I})} \left\{ \gamma_k \cdot \left[ \mathcal{L}_{\text{adv}} \cdot \frac{\sigma_k (\mathbf{r}^2 - 1)}{2\omega_k} \right. \right. \\ &\quad \left. \left. + \lambda \cdot \frac{(1 - 2 \cdot \tanh(\frac{\mu_k + \sigma_k \mathbf{r}}{\tau}) \cdot \frac{\sigma_k \mathbf{r}}{\tau})}{\sigma_k} \right] \right\}. \end{aligned} \quad (16)$$

The proof of Eq. (16) and the algorithm of DOP-DTA will be detailed in the Appendix. We use iterative gradient ascent to optimize the distribution parameters of each component. For each image, we first obtain the parameters of the multimodal distribution from the distribution mapping network as the initial values for optimization. Then, we iteratively perform gradient ascent to optimize the distribution parameters of each Gaussian component. As it is necessary to ensure that  $\sum_{k=1}^K \omega_k = 1$ , we perform normalization on  $\omega_k$  after each iteration.

## 3.5 Distribution-Based Adversarial Training

The concept of adversarial training (AT) traces back to the pioneering work of Goodfellow et al. [15], which is widely regarded as the most efficient approach to improving the robustness of deep learning models. Although prior work attempts to employ AT to bolster the models’ robustness against location-aware adversarial patches [16], [48], they incur an unacceptable overhead in producing a diverse set of adversarial samples. We posit that DOPatch can alleviate this issue owing to its ability to capture the distribution of adversarial locations, which endows it with the capacity to generate effective attacks and makes it a natural fit for AT. In this section, we discuss using DOPatch for distribution-based adversarial training (DOP-DMAT).

---

### Algorithm 2: Algorithms for DOP-DMAT

---

**Input:** dataset  $\mathcal{D}$ , distribution mapping network  $F_{\mathbf{W}}$ , target model  $f_{\tilde{h}}$ , training epochs  $N$ , components number  $K$ , Monte Carlo sample number  $Q$ , balance hyperparameter  $\lambda$ .

- 1 Initialize  $\mathbf{W}$  and  $\tilde{h}$ ;
- 2  $\{\omega_k\}_{k=1}^K \leftarrow \frac{1}{K}$ ;
- 3 **for** epoch = 1 **to**  $N$  **do**
- 4     **for** each minibatch  $\mathcal{B} \subset \mathcal{D}$  **do**
- 5         /\* inner maximization: \*/
- 6          $\{\mu_k^*, \sigma_k^*\}_{k=1}^K \leftarrow F_{\mathbf{W}}(\mathcal{B})$ ;
- 7          $\mathcal{L} \leftarrow 0$ ;
- 8         **for** q = 1 **to**  $Q$  **do**
- 9              $\mathcal{L} \leftarrow \mathcal{L} + \frac{1}{Q} (\mathcal{L}_{\text{adv}}(\mathcal{B}) - \lambda \cdot \mathcal{L}_{\text{entropy}})$ ;
- 10         **end**
- 11          $\mathbf{W} \leftarrow \mathbf{W} + \nabla_{\mathbf{W}} \mathcal{L}$ ;
- 12         /\* outer minimization: \*/
- 13         sample adversarial location  $\theta$  according to Eq. (4);
- 14         generate a set of  $(\mathbf{X}^{\text{adv}}, y') \in \mathcal{B}^{\text{adv}}$ ;
- 15          $\tilde{h} \leftarrow \tilde{h} + \nabla_{\tilde{h}} \mathcal{L}_{\text{adv}}(\{\mathcal{B}^{\text{adv}}, \mathcal{B}\})$ ;
- 16     **end**
- 17 **end**

**Output:** improved target model  $f_{\tilde{h}}$

---

Formally, DOP-DMAT is formulated as a distribution-based min-max optimization problem:

$$\min_{\tilde{h}} \max_{\mathbf{W}} \left[ \mathbb{E}_{\mathcal{N}(\mathbf{r}|0,\mathbf{I})} (\mathcal{L}_{\text{adv}} - \lambda \cdot \mathcal{L}_{\text{entropy}}) \right], \quad (17)$$

where  $\tilde{h}$  is the weight of the target model  $f_{\tilde{h}}(\cdot)$ . As shown in Eq. (17), we use DOPatch to solve the inner maximization problem, seeking the worst-case distribution of adversarial patch locations while maximizing both the adversarial loss and entropy regularization loss. The outer minimization aims to optimize the weights of the target model to minimize the expected loss on the worst-case distribution. Solving min-max problems directly is usually challenging. Based on Danskin’s theorem [10], a general solution is first to solve the inner problem to generate adversarial samples and then use gradient descent to solve the outer problem. For DOP-DMAT, we first optimize the distribution mapping network  $F_{\mathbf{W}}$  in each iteration, then sample alternative locations using Monte Carlo sampling after obtaining the current adversarial distribution. We then feed the generated adversarial patch samples with clean samples to update the weights of target model  $f_{\tilde{h}}$ . Algorithm 2 shows the training process of DOP-DMAT in a single iteration cycle.

## 4 EXPERIMENTS

### 4.1 Experimental Settings

**Datasets.** We evaluate our method on various public face datasets: LFW [20] and CelebA [32]. These datasets contain face images from 5749 and 8192 identities, respectively, and all images are used to construct the corresponding identity databases. We randomly select 1000 images for each dataset to perform impersonation attacks.

**Target Models.** We conduct experiments on various face recognition models, which span different backbone structures and training paradigms: FaceNet [39] with Inception-ResNet-v2, ArcFace [11] with IResNet-18, CosFace [47] with IResNet-18, SphereFace [30] with IResNet-50 and MobileFaceNet [7] with MobileNet-v2. We obtain the pre-training model separately from open-source projects<sup>1 2 3 4</sup>, each model obtain over 99% verification accuracy on LFW image pairs by following its optimal threshold. Following the settings in [48] and [16], we utilize these models to perform the attack on face classification and identification tasks. For the identification task, we use the pre-trained model as a feature extractor to obtain embeddings of face images, then select its nearest neighbor among all identities in the dataset as the prediction result. For the classification task, we add a fully connected layer after the aforementioned open-source models and fine-tune it on the target dataset until convergence. Then, we use the trained classifier to obtain the top-1 prediction for face images.

**Compared methods.** As our method improves location-aware patch attacks, we select the current state-of-the-art method, RHDE [16], [48], as the primary baseline. We also choose GDPA [27] as another comparative baseline and set a fixed pattern for GDPA while only optimizing for adversarial locations. In addition, two potential baselines are also considered, where adversarial locations are the mean location on the distribution optimized by DOPatch and directly transferred to attack other black-box models. This operation actually perform a transfer-based attack, which is named **DOP**. Based on DOPatch, we can also conduct the query-based attack, but a random sample from the distribution prior, which is named **DOP-Rd**. For adversarial training, we mainly compare standard training, data augmentation using randomly placed patches (Random-Aug), and a SOTA method AT method for adversarial patches [27].

**Evaluation metrics.** Regarding the attacks, we use the attack success rate (ASR) and the number of queries (NQ) as evaluation metrics. The former refers to the percentage of successfully attacked samples within the query limit among all the attacked samples. The latter refers to the average number of queries for all attacked samples. For adversarial training, we evaluate the attack success rate of the model under five location-aware patch methods.

**Implementation Details.** In experiments, we set the default values for the Gaussian component number as  $K = 5$  and the entropy regularization strength as  $\lambda = 0.1$ . The effects of these parameters are reported in Sec. 4.2. We employ FaceNet, SphereFace, and MobileFaceNet as the surrogate

models used in the first-stage optimization, respectively, for obtaining the adversarial distribution prior. The remaining models served as the target models for the black-box attacks. Specifically, for FaceNet and MobileNet, we utilize a combination structure of three residual blocks following the approach proposed in [54] as the feature extraction backbone for the distribution mapping network. While for SphereFace, we utilize the ResNet-50 [19] pre-trained on the CASIA-Webface dataset as the backbone. During the distribution-mapping network training, we adopt the Adam optimizer with an initial learning rate of 0.01 for training 500 epochs, and the learning rate decayed by a factor of 0.2 for every 150 epochs. In the DOP-LOA algorithm, the initial number of samples for Bayesian optimization is set to 10, and the maximum number of queries is set to 500. For the DOP-DTA algorithm, we set the learning rate of NES to 100, the population size to 10, and the maximum number of iterations to 50. Finally, the slope parameter of the  $\tanh(\cdot)$  function is set to  $\tau = 3000$ .

### 4.2 Ablation Studies

**Convergence under different  $\lambda$ .** For the optimization process of the distribution prior, i.e., in DOPatch, we conduct experiments to investigate the convergence of the distribution mapping network under different loss balance parameters  $\lambda$ . We plot the adversarial and entropy regularization loss curves during iteration, as shown in Fig. 4. Using FaceNet as the surrogate model, the distribution mapping network converges effectively when  $\lambda < 1.0$ , and the adversarial loss converges to the maximum when  $\lambda = 0.1$  and 0.01, indicating the optimized distribution prior is best in attack performance. Furthermore, a larger entropy regularization loss indicates that DOPatch can capture a more comprehensive adversarial region, which improves the performance of transfer attacks. In conclusion, we consider DOPatch to exhibit the best convergence performance when lambda is set to 0.1.

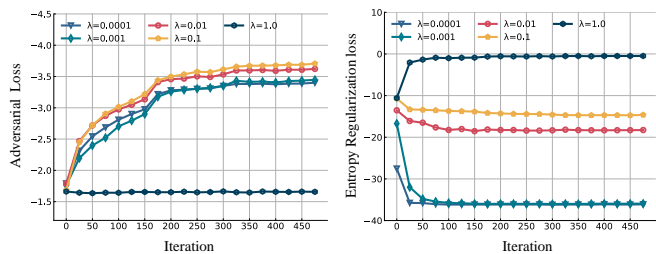


Fig. 4. Convergence curves of the adversarial loss and the entropy regularization loss with different values of  $\lambda$  (1.0, 0.1, 0.01, 0.001, and 0.0001) for FaceNet as the surrogate model.





**Effect of different surrogate models.** We utilize FaceNet, SphereFace, and MobileFaceNet as surrogate models, respectively, to investigate the impact of the obtained distribution prior on the attack performance across different surrogate models. Fig. 5 presents the attack success rates of DOP-LOA and DOP-DTA with adversarial distribution priors using different surrogate models. The results demonstrate that using FaceNet as the surrogate model achieves the best performance, which can be attributed to the superior cross-model transfer capability of the adversarial distribution

1. <https://github.com/timesler/facenet-pytorch>
2. <https://github.com/deepinsight/insightface/tree/master/recognition>
3. [https://github.com/wujiyang/Face\\_Pytorch](https://github.com/wujiyang/Face_Pytorch)
4. [https://github.com/Xiaooccer/MobileFaceNet\\_Pytorch](https://github.com/Xiaooccer/MobileFaceNet_Pytorch)



TABLE 1

The attack results of our method under different fixed patterns are presented. We select various cartoon stickers, the pattern generated by LaVAN [22] and random Gaussian noise as fixed patterns. By using FaceNet as the surrogate model, we perform black-box attacks on the remaining models. The attack success rate (ASR) and the number of queries (NQ) are reported.

Pattern	Method	FaceNet		SphereFace		MobileFaceNet		ArcFace		CosFace	
		ASR $\uparrow$	NQ $\downarrow$	ASR $\uparrow$	NQ $\downarrow$	ASR $\uparrow$	NQ $\downarrow$	ASR $\uparrow$	NQ $\downarrow$	ASR $\uparrow$	NQ $\downarrow$
	DOP-Rd	83.5%	219	36.6%	1783	83.4%	239	28.1%	2617	35.7%	1863
	DOP-LOA	<b>84.3%</b>	<b>110</b>	44.5%	640	90.6%	73	36.7%	895	47.4%	579
	DOP-DTA	83.0%	142	<b>61.9%</b>	<b>392</b>	<b>96.2%</b>	<b>71</b>	<b>53.2%</b>	<b>571</b>	<b>65.5%</b>	<b>371</b>
	DOP-Rd	88.2%	167	55.5%	870	95.1%	90	46.1%	1274	56.3%	867
	DOP-LOA	78.9%	<b>149</b>	46.1%	609	96.9%	<b>31</b>	39.1%	817	43.0%	710
	DOP-DTA	79.9%	167	<b>62.2%</b>	<b>388</b>	<b>97.1%</b>	70	<b>52.7%</b>	<b>563</b>	<b>62.6%</b>	<b>377</b>
	DOP-Rd	82.9%	226	27.1%	2764	38.8%	1670	43.6%	1338	91.2%	128
	DOP-LOA	82.8%	<b>115</b>	30.5%	1171	39.8%	814	46.1%	597	94.5%	<b>42</b>
	DOP-DTA	79.3%	169	<b>49.1%</b>	<b>648</b>	<b>64.8%</b>	<b>359</b>	<b>66.6%</b>	<b>320</b>	<b>96.7%</b>	63
	DOP-Rd	35.6%	1812	18.6%	4377	58.3%	721	25.5%	2933	20.8%	3811
	DOP-LOA	30.5%	1141	25.0%	1505	55.5%	407	31.3%	<b>1104</b>	23.4%	1640
	DOP-DTA	<b>72.2%</b>	<b>392</b>	<b>37.9%</b>	<b>1094</b>	<b>86.1%</b>	<b>210</b>	<b>31.7%</b>	1204	<b>29.9%</b>	<b>1405</b>

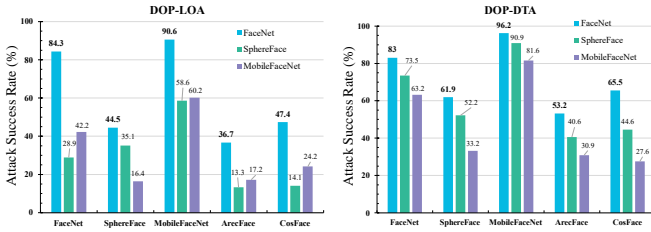


Fig. 5. **Attack success rates** of DOP-LOA and DOP-DTA against different face classifiers. FaceNet, SphereFace, and MobileFaceNet serve as surrogate models, respectively.

associated with FaceNet, allowing it to generalize across multiple models’ adversarial regions.

**Effect of different  $K$  values.** DOPatch parametrizes the adversarial region as a multimodal Gaussian distribution to capture a more comprehensive set of adversarial locations. Therefore, we further investigate the impact of different Gaussian component numbers on the performance of the proposed method. We set the number of components to  $K=1, 3, 5, 10,$  and  $15,$  then optimize the distribution prior under the LFW dataset and use FaceNet as the surrogate model. Fig. 6 demonstrates the attack success rates and query numbers of DOP-Rd, DOP-LOA, and DOP-DTA against ArcFace and CosFace in the face classification task. We observe that for the proposed query-based attack methods, the ASR increases while the corresponding NQ decreases as the number of Gaussian components  $K$  used in optimizing the distribution prior increases. This phenomenon is particularly prominent for  $K = 1$  to  $5$  and becomes less pronounced for  $K > 5,$  where ASR and NQ show relatively smooth variations w.r.t  $K$  increases. Furthermore, among different  $K$  settings, the proposed DOP-DTA achieves the best performance in terms of ASR and NQ, followed by DOP-LOA, while both methods outperform DOP-Rd significantly.

**Effect of different patterns.** We further conducted experiments using patches with different patterns. We selected three types of patterns: cartoon stickers, adversarial patches generated by LaVAN [22], and the Gaussian random noise. Table 1 present the ASR and NQ of the transfer attacks

against various face classifiers using FaceNet as the surrogate model. The results demonstrate the effectiveness of DOPatch in conducting attacks with different patterns. Moreover, meaningful patterns (cartoon stickers) yield better attack performance than meaningless textures (adversarial patches and Gaussian noise). Additionally, in most cases, DOP-DTA exhibits the best attack performance.

### 4.3 Attack Results on Face Classification Task

Table 2 presents the experimental results on the face classification task, where we compare the state-of-the-art methods, GDPA and RHDE. For our proposed methods (i.e., DOP, DOP-Rd, DOP-LOA, and DOP-DTA), we utilize FaceNet as the surrogate model. Based on the results, We have the following findings: **1)** The proposed DOPatch method achieves superior attack performance compared to both the white-box attack method (GDPA) and the black-box attack method (RHDE). It achieves the highest attack success rate against all five face classification models on both LFW and CelebA datasets. Moreover, compared to RHDE, DOPatch significantly improves attack efficiency with fewer required attack queries, which is mainly attributed to the ability of DOPatch to learn the underlying distribution of adversarial locations from the surrogate model and leverage its significant transferability. **2)** Compared to random sampling from the distribution prior (DOP-Rd), the proposed transfer-attack methods, Location Optimization Attack (DOP-LOA), and Distribution Transfer Attack (DOP-DTA) achieve higher attack success rates. However, DOP-LOA notably improves attack efficiency by reducing the number of queries while maintaining a high attack performance. In contrast, DOP-DTA aims to transfer the distribution prior to black-box models, resulting in higher attack success rates but requiring more queries compared to DOP-LOA. We selected some visualization samples of attacks, which are shown in Fig. 7.

### 4.4 Attack Results on Face Identification Task

Face identification is a widely used technique in the face recognition task, which searches for the most similar face in the database to determine the identity of the input face image. To verify the proposed method, we conduct digital

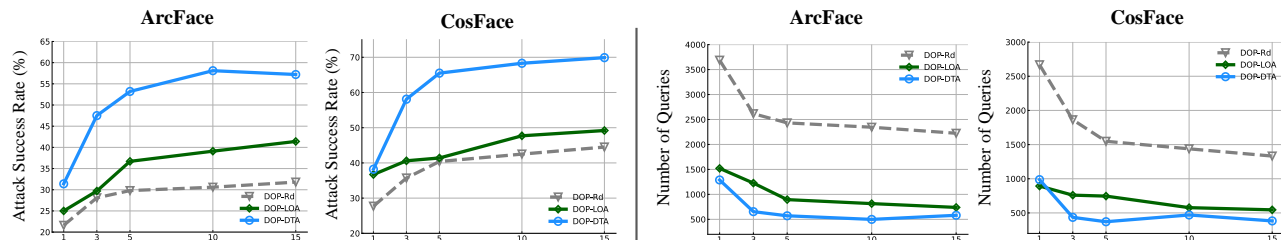


Fig. 6. Attack success rate and the number of query curves for DOP-Rd, DOP-LOA, and DOP-DTA using  $K$  ranging from 0 to 15.

TABLE 2

Attack performance evaluation on the LFW and CelebA datasets against **face classification** models. The table presents the attack success rate (ASR) and number of queries (NQ) using different location-aware methods against FaceNet, SphereFace, MobileFaceNet, ArcFace, and CosFace.

Method	LFW-1000subset [20]					CelebA-1000subset [32]														
	FaceNet		SphereFace		MobileFaceNet		ArcFace		CosFace		FaceNet		SphereFace		MobileFaceNet		ArcFace		CosFace	
	ASR $\uparrow$	NQ $\downarrow$	ASR $\uparrow$	NQ $\downarrow$	ASR $\uparrow$	NQ $\downarrow$	ASR $\uparrow$	NQ $\downarrow$	ASR $\uparrow$	NQ $\downarrow$	ASR $\uparrow$	NQ $\downarrow$	ASR $\uparrow$	NQ $\downarrow$	ASR $\uparrow$	NQ $\downarrow$	ASR $\uparrow$	NQ $\downarrow$	ASR $\uparrow$	NQ $\downarrow$
Clean	0.1%	-	0.0%	-	0.2%	-	1.1%	-	0.8%	-	6.6%	-	13.3%	-	13.3%	-	13.9%	-	8.3%	-
GDPA [27]	53.0%	-	30.4%	-	57.7%	-	25.5%	-	20.6%	-	49.8%	-	47.6%	-	57.3%	-	42.8%	-	38.6%	-
RHDE [48]	42.2%	1945	31.3%	2950	65.9%	801	43.7%	1743	61.6%	920	74.3%	631	74.6%	558	72.9%	621	61.4%	894	65.5%	796
DOP	72.6%	-	23.1%	-	52.4%	-	12.7%	-	17.5%	-	50.2%	-	40.2%	-	56.9%	-	40.4%	-	37.5%	-
DOP-Rd	83.5%	219	36.6%	1783	83.4%	239	28.1%	2617	35.7%	1863	89.3%	149	77.6%	327	91.5%	118	74.5%	388	64.0%	601
DOP-LOA	<b>84.3%</b>	<b>110</b>	44.5%	639	90.6%	73	36.7%	895	47.4%	579	<b>93.0%</b>	<b>61</b>	78.9%	<b>145</b>	<b>92.2%</b>	<b>55</b>	77.3%	<b>168</b>	63.3%	312
DOP-DTA	83.0%	142	<b>61.9%</b>	<b>392</b>	<b>96.2%</b>	<b>71</b>	<b>53.2%</b>	<b>571</b>	<b>65.5%</b>	<b>371</b>	82.2%	145	<b>79.6%</b>	178	90.2%	91	<b>78.7%</b>	196	<b>69.5%</b>	<b>286</b>

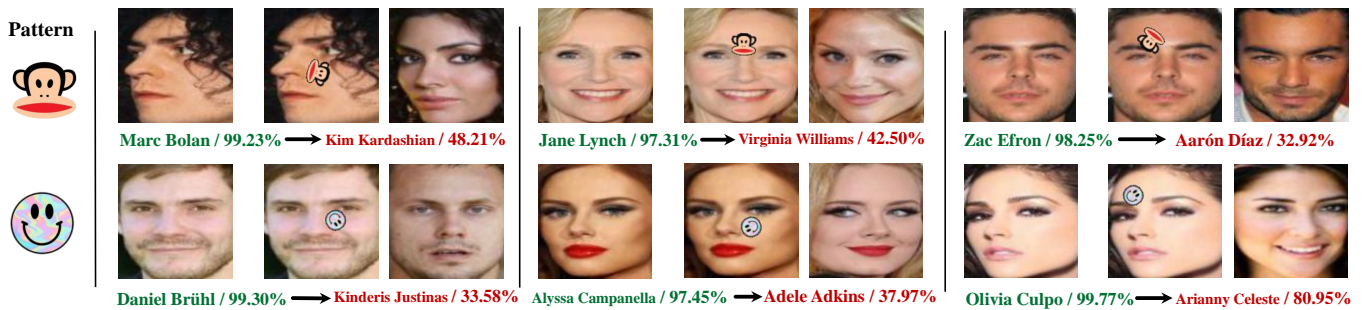


Fig. 7. Examples of attacks using various patterns. Each group showcases the original face image, the face image post-attack, and the face image of the misclassified class. The correct identity is highlighted in green text, while the predicted wrong identity after the attack is marked in red text. The accompanying percentages indicate the confidence values of the predicted results.

and physical attacks versus face identification, respectively. Specifically, we regard all the face images in LFW as the database and manipulate some query face images to perform impersonation attacks. The attack is successful if the returned identity is different from the query image. We adopt the same face identification setting with [48]. Table 3 lists the experimental results of digital attacks against face identification using FaceNet, ArcFace, and CosFace. We can see that DOP-LOA and DOP-DTA significantly outperform RHDE for all the threat models versus ASR and NQ, showing that the distribution prior is indeed effective for query-based attacks. In addition, DOP-DTA is better than DOP-LOA, showing the superiority of distributional modeling.

Besides, we also give physical attacks against face identification. We add a reference face image of a volunteer into the CelebA database, and then paste the sticker on the volunteer’s face according to the results of DOP-DTA. Finally, we use a camera to shoot the volunteer’s face. The

TABLE 3

Digital attack performance evaluation on the LFW dataset against **face identification** models. The table presents the attack success rate (ASR) and number of queries (NQ) using different location-aware methods against FaceNet, ArcFace and CosFace.

Method	LFW-1000subset [20]					
	FaceNet		ArcFace		CosFace	
	ASR $\uparrow$	NQ $\downarrow$	ASR $\uparrow$	NQ $\downarrow$	ASR $\uparrow$	NQ $\downarrow$
Clean	0.1%	-	0.1%	-	0.1%	-
GDPA [27]	10.9%	-	17.5%	-	17.3%	-
RHDE [48]	48.8%	1666	35.4%	2695	42.9%	2136
DOP	31.5%	-	13.1%	-	14.9%	-
DOP-Rd	56.1%	839	38.0%	1718	43.3%	1409
DOP-LOA	54.7%	<b>447</b>	34.4%	988	44.5%	676
DOP-DTA	<b>56.1%</b>	515	<b>59.5%</b>	<b>492</b>	<b>60.7%</b>	<b>507</b>

captured manipulated face image is then used to perform face identification. To verify the robustness of our DOPatch, we test the attack performance under different angles (rota-

TABLE 4

Attacks on ImageNet against **image recognition** models: VGG-16, Inception-v3 (Inc-v3), ResNet-50 (Res-50), MobileNet-v2 (MN-v2), ViT-Base (ViT-B/16), SwinTransformer-Tiny (Swin-T) and CLIP (Zero-Shot). Inception-v3 is utilized as the surrogate model (ACC denotes Accuracy).

Method	VGG-16		Inc-v3		Res-50		MN-v2		ViT-B/16		Swin-T		CLIP (Zero-Shot)	
	ACC ↓	NQ ↓	ACC ↓	NQ ↓	ACC ↓	NQ ↓	ACC ↓	NQ ↓	ACC ↓	NQ ↓	ACC ↓	NQ ↓	ACC ↓	NQ ↓
Clean	69.9%	-	66.9%	-	68.8%	-	75.4%	-	78.2%	-	78.9%	-	67.3%	-
DOP-LOA	34.4%	301	28.9%	221	47.7%	472	35.2%	294	69.5%	1152	64.1%	927	40.6%	347
DOP-DTA	22.5%	191	17.6%	154	27.5%	245	21.7%	179	61.4%	884	54.3%	663	39.1%	360

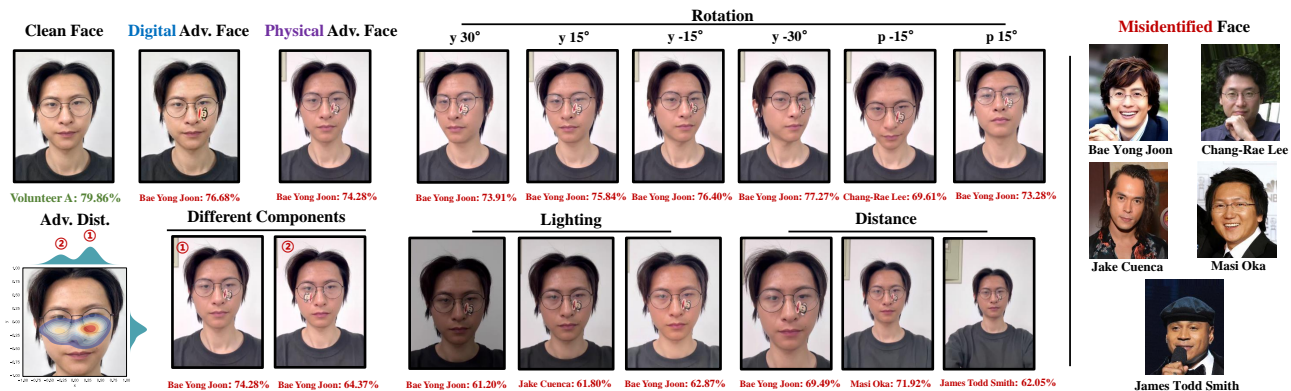


Fig. 8. Qualitative results of **physical attacks** against face identification under different angles, distances, lighting, and locations.

TABLE 5

Quantitative results of **physical attacks** against face identification under different angles, distances and lighting.

	0°	yaw ±15°	yaw ±30°	pitch ±15°	distance	lighting
ASR	85.42%	79.31%	56.52%	60.38%	60.42%	62.82%

tion), distances and lighting of the camera. The qualitative results are given in Fig. 8. Our DOP-DTA shows good attack ability under different physical changes, demonstrating its effectiveness in the real world. The quantitative results are given in Table 5, where we see that DOP-DTA achieves more than 50% ASR under all the settings, a satisfactory physical attack performance.

#### 4.5 Attack Results on Image Recognition Task

We further extend DOPatch to the image recognition task and conduct attack experiments on the ImageNet dataset. Specifically, we use classifiers pre-trained on ImageNet-1K as the target models, including CNN-based models VGG-16, Inception-v3, ResNet-50, and MobileNet-v2, as well as Transformer-based models ViT-Base, SwinTransformer-Tiny and Clip model, all these classifiers use open-source weights from torchvision<sup>1</sup> and timm<sup>2</sup>. We randomly selected 1000 images from the ImageNet-1K test set to conduct the attacks. In the attack setup, we use Inception-v3 as the surrogate model and keep the other parameter settings consistent with Sec. 4.1. We evaluate the attack success rates and the number of queries of DOP-LOA and DOP-DTA on various classifiers, as shown in Tab. 4. After applying the attacks, the classification performance of the models is significantly degraded, demonstrating the effectiveness of DOPatch. Some

examples of the attacks are shown in Fig. 9. Furthermore, we observe that CNN-based models exhibit more noticeable performance degradation than Transformer-based models when facing DOPatch attacks, highlighting the robustness of Transformer-based models against patch perturbations.

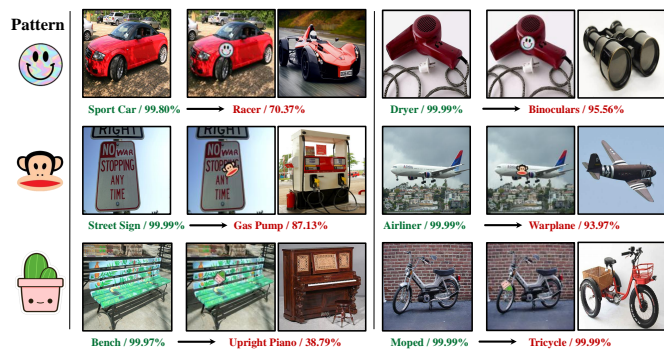


Fig. 9. Examples of DOPatch against Inception-v3 classifier. Each group includes the original image, the attacked image, and the image corresponding to the predicted wrong class after the attacks.

#### 4.6 Defense Results with Adversarial Training

Table 6 presents the performance of the proposed DOP-DMAT on the face classification task. We compare DOP-DMAT to a potential baseline, which involves using randomly positioned adversarial patch samples for data augmentation. Besides, we also compare with GDPA-AT [27], which utilizes a dynamic adversarial patch for both location and pattern to perform adversarial training. In our experimental setup, we first investigate the impact of  $K$  in the inner maximization process to adversarial training. The results are given in Table 7. From the table, we can see that when  $K = 5$ , DOP-DMAT achieves the best defensive performance, thus we fix  $K = 5$  to compare with other

1. <https://pytorch.org/vision/stable/index.html>

2. <https://github.com/huggingface/pytorch-image-models>

TABLE 6

Evaluation of **adversarial training** on face classification tasks using DOP-DMAT with FaceNet and ArcFace. Robustness is assessed based on the attack success rate (ASR) and the number of queries (NQ) under various attack methods. *max* denotes the maximum queries are used.

Method	FaceNet									ArcFace								
	Clean	RHDE [48]		GDPA [27]		DOP-LOA		DOP-DTA		Clean	RHDE [48]		GDPA [27]		DOP-LOA		DOP-DTA	
	ASR ↓	ASR ↓	NQ ↑	ASR ↓	NQ ↑	ASR ↓	NQ ↑	ASR ↓	NQ ↑	ASR ↓	ASR ↓	NQ ↑	ASR ↓	NQ ↑	ASR ↓	NQ ↑	ASR ↓	NQ ↓
Standard-Trained	0.1%	42.2%	1945	53.0%	-	84.3%	110	83.0%	142	1.1%	43.7%	1743	25.5%	-	36.7%	895	53.2%	571
Random-Aug	0.0%	21.2%	4929	19.9%	-	59.4%	447	31.4%	1131	0.0%	12.8%	8539	2.1%	-	7.8%	6560	2.2%	22450
GDPA-AT [27]	0.0%	11.4%	9725	2.5%	-	<b>0.8%</b>	<b>62018</b>	15.4%	3096	0.0%	18.8%	5453	1.0%	-	<b>0.0%</b>	<i>max</i>	<b>0.9%</b>	<b>55475</b>
DOP-DMAT	0.0%	<b>4.5%</b>	<b>26146</b>	<b>1.8%</b>	-	1.6%	30856	<b>6.0%</b>	<b>8334</b>	0.0%	<b>7.8%</b>	<b>12817</b>	<b>0.1%</b>	-	<b>0.0%</b>	<i>max</i>	1.4%	35950

TABLE 7

Attack performance of RHDE on FaceNet using DOP-DMAT with different values of  $K$ .

	$K=1$		$K=3$		$K=5$		$K=10$		$K=15$	
	ASR	NQ	ASR	NQ	ASR	NQ	ASR	NQ	ASR	NQ
RHDE	12.9%	8592	4.8%	24280	<b>4.5%</b>	<b>26146</b>	5.9%	19698	5.6%	21149

SOTA adversarial training methods in Table 6. The learning rate and lambda for the distribution mapping network are consistent with Sec. 4.1. We set the learning rate to 0.001 for the face classification models and trained for 150 epochs. We conduct experiments on FaceNet and ArcFace models under the LFW dataset, evaluating the trained models with the proposed DOP-LOA, DOP-DTA and two location-aware attack methods: RHDE [48] and GDPA [27]. We have the following findings based on the results: DOP-DMAT perform best in improving the model’s robustness against various location-aware patches compared to the random data augmentation and GDPA-AT that mainly utilize the individual locations to perform adversarial training, which can be attributed to DOP-DMAT’s ability to capture the worst-case distribution of adversarial locations, thereby enhancing the model’s robustness against these worst-case scenarios. Taking FaceNet as an example, after training by DOP-DMAT, the ASR of purely location-aware patches attack decreases from 42.2% to 5.6% (RHDE), 53.0% to 1.8% (GDPA), 84.3% to 1.6% (DOP-LOA) and 83.0% to 6.0% (DOP-DTA). Correspondingly, the query count also increases significantly.

## 5 CONCLUSION

In this paper, we have proposed a novel method for generating location-aware adversarial patches, called Distribution-Optimized Adversarial Patch (DOPatch). DOPatch optimized a multimodal distribution of adversarial locations instead of individual ones, which enabled efficient query-based black-box attacks via transfer prior, and robustness improvement via Distributional-Modeling Adversarial Training (DOP-DMAT). We have demonstrated the superiority and efficiency of DOPatch over existing methods on various face classification and recognition tasks. We have also provided insights into the distribution of adversarial locations and their relation to the model’s vulnerability. Our work has the potential to open up new possibilities for exploring and defending against location-aware adversarial patches in the physical world.

## REFERENCES

- [1] Andriushchenko, M., Croce, F., Flammarion, N., Hein, M.: Square attack: a query-efficient black-box adversarial attack via random search. In: ECCV. pp. 484–501 (2020)
- [2] Athalye, A., Engstrom, L., Ilyas, A., Kwok, K.: Synthesizing robust adversarial examples. In: International conference on machine learning. pp. 284–293. PMLR (2018)
- [3] Blundell, C., Cornebise, J., Kavukcuoglu, K., Wierstra, D.: Weight uncertainty in neural network. In: International conference on machine learning. pp. 1613–1622. PMLR (2015)
- [4] Brown, T.B., Mané, D., Roy, A., Abadi, M., Gilmer, J.: Adversarial patch. arXiv preprint arXiv:1712.09665 (2017)
- [5] Carlini, N., Wagner, D.: Towards evaluating the robustness of neural networks. In: 2017 IEEE Symposium on Security and Privacy (SP). pp. 39–57. Ieee (2017)
- [6] Chen, C., Huang, T.: Camdar-adv: generating adversarial patches on 3d object. International Journal of Intelligent Systems 36(3), 1441–1453 (2021)
- [7] Chen, S., Liu, Y., Gao, X., Han, Z.: Mobilefacenets: Efficient cnns for accurate real-time face verification on mobile devices. In: Biometric Recognition: 13th Chinese Conference, CCBR 2018, Urumqi, China, August 11–12, 2018, Proceedings 13. pp. 428–438. Springer (2018)
- [8] Chiang, P.y., Ni, R., Abdelkader, A., Zhu, C., Studer, C., Goldstein, T.: Certified defenses for adversarial patches. arXiv preprint arXiv:2003.06693 (2020)
- [9] Chindaudom, A., Siritanawan, P., Sumongkayothin, K., Kotani, K.: Adversarialqr: An adversarial patch in qr code format. In: 2020 Joint 9th International Conference on Informatics, Electronics & Vision (ICIEV) and 2020 4th International Conference on Imaging, Vision & Pattern Recognition (icIVPR). pp. 1–6. IEEE (2020)
- [10] Danskin, J.M.: The theory of max-min and its application to weapons allocation problems, vol. 5. Springer Science & Business Media (2012)
- [11] Deng, J., Guo, J., Xue, N., Zafeiriou, S.: Arcface: Additive angular margin loss for deep face recognition. In: Proceedings of the IEEE/CVF conference on computer vision and pattern recognition. pp. 4690–4699 (2019)
- [12] Dong, Y., Deng, Z., Pang, T., Zhu, J., Su, H.: Adversarial distributional training for robust deep learning. Advances in Neural Information Processing Systems 33, 8270–8283 (2020)
- [13] Dong, Y., Liao, F., Pang, T., Su, H., Zhu, J., Hu, X., Li, J.: Boosting adversarial attacks with momentum. In: Proceedings of the IEEE conference on computer vision and pattern recognition. pp. 9185–9193 (2018)
- [14] Eykholt, K., Evtimov, I., Fernandes, E., Li, B., Rahmati, A., Xiao, C., Prakash, A., Kohno, T., Song, D.: Robust physical-world attacks on deep learning visual classification. In: Proceedings of the IEEE conference on computer vision and pattern recognition. pp. 1625–1634 (2018)
- [15] Goodfellow, I.J., Shlens, J., Szegedy, C.: Explaining and harnessing adversarial examples. arXiv preprint arXiv:1412.6572 (2014)
- [16] Guo, Y., Wei, X., Wang, G., Zhang, B.: Meaningful adversarial stickers for face recognition in physical world. arXiv e-prints pp. arXiv-2104 (2021)
- [17] Gürel, N.M., Qi, X., Rimanic, L., Zhang, C., Li, B.: Knowledge enhanced machine learning pipeline against diverse adversarial attacks. In: International Conference on Machine Learning. pp. 3976–3987 (2021)

- [18] Hayes, J.: On visible adversarial perturbations & digital watermarking. In: Proceedings of the IEEE Conference on Computer Vision and Pattern Recognition Workshops. pp. 1597–1604 (2018)
- [19] He, K., Zhang, X., Ren, S., Sun, J.: Deep residual learning for image recognition. In: Proceedings of the IEEE conference on computer vision and pattern recognition. pp. 770–778 (2016)
- [20] Huang, G.B., Mattar, M., Berg, T., Learned-Miller, E.: Labeled faces in the wild: A database for studying face recognition in unconstrained environments. In: Workshop on faces in 'Real-Life' Images: detection, alignment, and recognition (2008)
- [21] Jaderberg, M., Simonyan, K., Zisserman, A., et al.: Spatial transformer networks. *Advances in neural information processing systems* **28** (2015)
- [22] Karmon, D., Zoran, D., Goldberg, Y.: Lavan: Localized and visible adversarial noise. In: International Conference on Machine Learning. pp. 2507–2515. PMLR (2018)
- [23] Kingma, D.P., Welling, M.: Auto-encoding variational bayes. arXiv preprint arXiv:1312.6114 (2013)
- [24] Komkov, S., Petiushko, A.: Advhat: Real-world adversarial attack on arcface face id system. In: 2020 25th International Conference on Pattern Recognition (ICPR). pp. 819–826. IEEE (2021)
- [25] Kurakin, A., Goodfellow, I.J., Bengio, S.: Adversarial examples in the physical world. In: Artificial intelligence safety and security, pp. 99–112. Chapman and Hall/CRC (2018)
- [26] Lee, M., Kolter, Z.: On physical adversarial patches for object detection. arXiv preprint arXiv:1906.11897 (2019)
- [27] Li, X., Ji, S.: Generative dynamic patch attack. *BMVC* (2021)
- [28] Liu, A., Liu, X., Fan, J., Ma, Y., Zhang, A., Xie, H., Tao, D.: Perceptual-sensitive gan for generating adversarial patches. In: Proceedings of the AAAI conference on artificial intelligence. vol. 33, pp. 1028–1035 (2019)
- [29] Liu, J., Levine, A., Lau, C.P., Chellappa, R., Feizi, S.: Segment and complete: Defending object detectors against adversarial patch attacks with robust patch detection. In: Proceedings of the IEEE/CVF Conference on Computer Vision and Pattern Recognition. pp. 14973–14982 (2022)
- [30] Liu, W., Wen, Y., Yu, Z., Li, M., Raj, B., Song, L.: Spheroface: Deep hypersphere embedding for face recognition. In: Proceedings of the IEEE conference on computer vision and pattern recognition. pp. 212–220 (2017)
- [31] Liu, X., Yang, H., Liu, Z., Song, L., Li, H., Chen, Y.: Dpatch: An adversarial patch attack on object detectors. arXiv preprint arXiv:1806.02299 (2018)
- [32] Liu, Z., Luo, P., Wang, X., Tang, X.: Large-scale celebfaces attributes (celeba) dataset. Retrieved August 15(2018), 11 (2018)
- [33] Madry, A., Makelov, A., Schmidt, L., Tsipras, D., Vladu, A.: Towards deep learning models resistant to adversarial attacks. arXiv preprint arXiv:1706.06083 (2017)
- [34] Metzger, J.H., Finnie, N., Huttmacher, R.: Meta adversarial training against universal patches. arXiv preprint arXiv:2101.11453 (2021)
- [35] Mirsky, Y.: Ipatch: A remote adversarial patch. arXiv preprint arXiv:2105.00113 (2021)
- [36] Naseer, M., Khan, S., Porikli, F.: Local gradients smoothing: Defense against localized adversarial attacks. In: 2019 IEEE Winter Conference on Applications of Computer Vision (WACV). pp. 1300–1307. IEEE (2019)
- [37] Nesti, F., Rossolini, G., Nair, S., Biondi, A., Buttazzo, G.: Evaluating the robustness of semantic segmentation for autonomous driving against real-world adversarial patch attacks. In: Proceedings of the IEEE/CVF Winter Conference on Applications of Computer Vision. pp. 2280–2289 (2022)
- [38] Rao, S., Stutz, D., Schiele, B.: Adversarial training against location-optimized adversarial patches. In: Computer Vision–ECCV 2020 Workshops: Glasgow, UK, August 23–28, 2020, Proceedings, Part V 16. pp. 429–448. Springer (2020)
- [39] Schroff, F., Kalenichenko, D., Philbin, J.: Facenet: A unified embedding for face recognition and clustering. In: Proceedings of the IEEE conference on computer vision and pattern recognition. pp. 815–823 (2015)
- [40] Sharif, M., Bhagavatula, S., Bauer, L., Reiter, M.K.: Accessorize to a crime: Real and stealthy attacks on state-of-the-art face recognition. In: Proceedings of the 2016 acm sigsac conference on computer and communications security. pp. 1528–1540 (2016)
- [41] Sharif, M., Bhagavatula, S., Bauer, L., Reiter, M.K.: A general framework for adversarial examples with objectives. *ACM Transactions on Privacy and Security (TOPS)* **22**(3), 1–30 (2019)
- [42] Snoek, J., Larochelle, H., Adams, R.P.: Practical bayesian optimization of machine learning algorithms. *Advances in neural information processing systems* **25** (2012)
- [43] Sun, Y., Wang, X., Tang, X.: Deep learning face representation from predicting 10,000 classes. In: Proceedings of the IEEE conference on computer vision and pattern recognition. pp. 1891–1898 (2014)
- [44] Szegedy, C., Zaremba, W., Sutskever, I., Bruna, J., Erhan, D., Goodfellow, I., Fergus, R.: Intriguing properties of neural networks. arXiv preprint arXiv:1312.6199 (2013)
- [45] Taigman, Y., Yang, M., Ranzato, M., Wolf, L.: Deepface: Closing the gap to human-level performance in face verification. In: Proceedings of the IEEE conference on computer vision and pattern recognition. pp. 1701–1708 (2014)
- [46] Thys, S., Van Ranst, W., Goedemé, T.: Fooling automated surveillance cameras: adversarial patches to attack person detection. In: Proceedings of the IEEE/CVF conference on computer vision and pattern recognition workshops. pp. 0–0 (2019)
- [47] Wang, H., Wang, Y., Zhou, Z., Ji, X., Gong, D., Zhou, J., Li, Z., Liu, W.: Cosface: Large margin cosine loss for deep face recognition. In: Proceedings of the IEEE conference on computer vision and pattern recognition. pp. 5265–5274 (2018)
- [48] Wei, X., Guo, Y., Yu, J.: Adversarial sticker: A stealthy attack method in the physical world. *IEEE Transactions on Pattern Analysis and Machine Intelligence* **45**(3), 2711–2725 (2023)
- [49] Wei, X., Guo, Y., Yu, J., Zhang, B.: Simultaneously optimizing perturbations and positions for black-box adversarial patch attacks. *IEEE Transactions on Pattern Analysis and Machine Intelligence* **45**(7), 9041–9054 (2023)
- [50] Xiang, C., Bhagoji, A.N., Sehwal, V., Mittal, P.: Patchguard: A provably robust defense against adversarial patches via small receptive fields and masking. In: USENIX Security Symposium. pp. 2237–2254 (2021)
- [51] Yamanaka, K., Matsumoto, R., Takahashi, K., Fujii, T.: Adversarial patch attacks on monocular depth estimation networks. *IEEE Access* **8**, 179094–179104 (2020)
- [52] Yang, C., Kortylewski, A., Xie, C., Cao, Y., Yuille, A.: Patchattack: A black-box texture-based attack with reinforcement learning. In: Computer Vision–ECCV 2020: 16th European Conference, Glasgow, UK, August 23–28, 2020, Proceedings, Part XXVI. pp. 681–698. Springer (2020)
- [53] Yang, X., Liu, C., Xu, L., Wang, Y., Dong, Y., Chen, N., Su, H., Zhu, J.: Towards effective adversarial textured 3d meshes on physical face recognition. arXiv preprint arXiv:2303.15818 (2023)
- [54] Zhu, J.Y., Park, T., Isola, P., Efros, A.A.: Unpaired image-to-image translation using cycle-consistent adversarial networks. In: Proceedings of the IEEE international conference on computer vision. pp. 2223–2232 (2017)
- [55] Zolfi, A., Avidan, S., Elovici, Y., Shabtai, A.: Adversarial mask: Real-world adversarial attack against face recognition models. arXiv preprint arXiv:2111.10759 (2021)